Available online at www.sciencedirect.com
SCIENCE DIRECT®
ELSEVIER
Journal of Magnetism and Magnetic Materials 278 (2004) 348–358
Journal of magnetism and magnetic materials
www.elsevier.com/locate/jmmm

The effect of the magnetic field on the corrosion behavior of Nd–Fe–B permanent magnets

I. Costa[a,*], M.C.L. Oliveira[a], H.G. de Melo[b], R.N. Faria[a]

[a] *Instituto de Pesquisas Energéticas e Nucleares, IPEN-CNEN-SP, Av. Prof. Lineu Prestes, 2242, São Paulo CEP 05508-900, SP, Brazil*
[b] *Escola Politécnica da USP, Departamento de Engenharia Química, Av. Prof. Lineu Prestes, Trav. 3, no. 380, São Paulo CEP 05508-900, SP, Brazil*

Received 15 August 2003; received in revised form 10 December 2003

Abstract

The effect of magnetic field on the corrosion behavior of an Nd–Fe–B magnet has been investigated in a naturally aerated 3.5 wt% sodium chloride solution. Experimentally, the study was carried out by weight loss, electrochemical impedance spectroscopy and potentiodynamic polarization tests. The results have shown an evident effect of the magnetization state on the corrosion behavior of the Nd–Fe–B specimens. Magnetized specimens exhibited larger weight losses than non-magnetized ones. The difference in the specimens' corrosion rates were ascribed to the effect of the magnetic field on the transport of oxygen in the solution to the magnet/electrolyte interface, evidenced in the high-frequency response of the impedance diagrams, and to the adherence of particles to the magnetized specimens' surface due to magnetic field. Attempts have been made to explain the corrosion behavior observed for magnetized and non-magnetized sintered magnets.

PACS: 81.70.−q; 82.45.+z; 82.80.Fk

Keywords: Nd–Fe–B magnets; Corrosion; Magnetic field; Electrochemical techniques

1. Introduction

Aqueous corrosion is an electrochemical process where high interfacial electric field is involved. As it is well documented, this property is influenced by the existence of a magnetic field [1–16]. Therefore, when a magnetized sample is submitted to an aggressive medium, an influence of the magnetic field in its corrosion rate must be expected, and, hence, corrosion rates in the presence of a magnetic field should differ from that in field-free environment.

In the literature, the reported effects of magnetic field in the corrosion behavior of metals are controversial. Several authors have reported that magnetic fields decrease the corrosion rates of metals [1–6]. Some examples are the decrease in copper and iron corrosion rates in nitric acid solution under constant magnetic field [1], the lowering of the corrosion of pure iron in sulphate

*Corresponding author. CCTM-Corrosion Laboratory, IPEN-CNEN-SP, Av. Prof. Lineu Prestes, 2242, Cid 05508000 São Paulo, SP, Brazil. Tel.: +55-11-38169356; fax: +55-11-38169370.
E-mail address: icosta@ipen.br (I. Costa).

0304-8853/$ - see front matter © 2004 Elsevier B.V. All rights reserved.
doi:10.1016/j.jmmm.2003.12.1320

and chloride solutions [2,3], and the inhibiting effect exerted by the field in the corrosion of zinc, brass and aluminum [4,5] and in the corrosion of AISI 303 stainless steel in $FeCl_3$ solution [6]. In this latter case, the inhibitory effect was explained in terms of the development of a field-assisted passive layer. Conversely, it has also been reported that magnetic field increases the corrosion rate of some metallic materials such as titanium in sulphate solutions [7]. An accelerating effect of the magnetic field has also been observed on the cathodic reaction of the single corrosion process related to AISI 303 SS in $FeCl_3$ solution, i.e., reduction of Fe^{3+} to Fe^{2+} [6].

According to the literature, a magnetic field can influence metallic corrosion by acting on the electrode kinetics [8,9], on the mass transport [10–16], on the formation of an interfacial oxide/hydroxide layer [3–6] or on the potential difference at the metal/solution interface [7].

Most of the studies on the effects of magnetic fields on metallic corrosion have been carried out with flux densities ranging from 0.05 to 1.5 T. In these studies, fields were applied either by a magnet next to the electrode [6] or by placing the electrochemical cell in the gap of an electromagnet [17]. On the other hand, only few works have been carried out on the effect of magnetization state on the corrosion of magnetically hard rare-earth-based materials [18–21].

According to Bala, the state of magnetization hardly affects the corrosion of $SmCo_5$ magnets [18,19]. These authors also reported that Nd–Fe–B magnets in the magnetized state undergo lower dissolution under cathodic polarization, as compared to non-magnetized samples, and this was called abnormal dissolution [20]. However, it has also been pointed out that the surface degradation of a magnetized $Nd_{16}Fe_{77}B_8$ permanent magnet was as high as in the case of a non-magnetized one, and that weight losses associated with this type of magnet hardly differed for both states of magnetization [20]. Conversely, previous works carried out in our laboratory indicated that the state of magnetization of an Nd–Fe–B permanent magnet affects its corrosion performance [21]. The present paper reports the results of further work carried out on this subject for Nd–Fe–B-type magnets using electrochemical methods and weight loss measurements. Based on the experimental results, a corrosion mechanism has been proposed, taking into account the influence of magnetization and surface states of the samples.

2. Experimental procedure

2.1. Material

Due to the high number of samples needed to perform all the experiments, and in order to maintain sample uniformity during the whole procedure, commercial sintered Nd–Fe–B magnets produced by Crucible were used in this investigation. The magnet composition, given in Table 1, was determined by X-ray fluorescence analysis and atomic absorption measurements. The corrosion behavior of the magnets was investigated in naturally aerated 3.5 wt% NaCl solution. In all the tests, solutions were quiescent and the temperature was in the range of $23 \pm 2^{\circ}C$. Magnetization of samples was carried out up to saturation in a pulsed field of 60 kOe, and all the tests were performed with magnetized and non-magnetized samples.

2.2. Specimen preparation for electrochemical measurements

Electrodes with an approximate transversal area of 130 mm^2 were prepared by cold resin mounting. Before testing, the electrode surfaces were ground

Table 1
Chemical composition (wt%) of commercial Nd–Fe–B magnets

Elem.	Fe	Nd	B	Dy	Al	Co	Si	Cu	Nb	Na	S
%	60.6	28.3	1.0	2.1	3.7	1.3	1.4	0.2	0.2	0.4	0.2

with silicon carbide paper up to grade #1000, followed by degreasing with acetone, using an ultrasonic bath, rinsing with deionized water and drying under a hot air stream. Magnetization was carried out after surface preparation.

2.3. Experimental set-up and conditions of electrochemical tests

A three-electrode cell arrangement was used for the electrochemical measurements, with a graphite rod and a saturated calomel (SCE) as counter and reference electrodes, respectively. Electrochemical impedance spectroscopy (EIS) measurements were accomplished with a 1255 Solartron frequency response analyzer coupled to an EG&G 273A Potentiostat. All EIS measurements were performed in potentiostatic mode and at the corrosion potential (E_{corr}). The amplitude of the perturbation signal was 10 mV, and the investigated frequency range varied from 10^5 to 10^{-2} Hz with an acquisition rate of 7 points per decade. Potentiodynamic polarization measurements were carried out using an EG&G 273A Potentiostat coupled to a computer. The investigated potential range was from −1300 (SCE) to 0 mV (SCE), with a scan rate of 1 mV/s. Electrochemical measurements were obtained at increasing test times, from 1 until 60 days of immersion.

2.4. Weight loss measurements

For weight loss measurements, magnets ($\varnothing = 12.5$ mm and $l = 6$ mm) were submitted to the same surface treatment used in the electrochemical tests and their areas measured. Subsequently, the sample surfaces were degreased with acetone using an ultrasonic bath, rinsed with deionized water and dried under a hot air stream. Next, the specimens were weighed using an analytical balance Shimadzu Libror AEL-40SM. Some samples were magnetized (after surface preparation and weighing) up to saturation with a pulsed field of 60 kOe. After weighing, the samples were immersed in the test solution and at immersion periods corresponding to 5, 15, 20, 30, 40, and 60 days. At each interval, six magnetized and six non-magnetized samples were removed from the solution for weighing. The loose corrosion products were then removed by brushing the sample surfaces with a soft brush, followed by rinsing with deionized water and drying under a hot air stream. After drying, all the samples were weighed and then heat treated in a furnace at 400°C for 30 min. This heat treatment was carried out for demagnetization of the previously magnetized samples. However, to avoid introducing different conditions in the various samples tested, magnetized and non-magnetized samples were heat treated. As the heat treatment caused the release of particles from the magnetized samples, all the samples and released particles were weighed after the heat treatment step.

2.5. Demagnetization curves

The magnetic properties of corrosion-tested specimens were determined before and after increasing times of test, in a permeameter. Measurements were performed after saturation in a pulsed field of 60 kOe.

2.6. SEM imaging

Scanning electron microscopy of the magnet surfaces after increasing the times of test was carried out using a Philips XL-30 microscope.

3. Results

The weight loss results for the non-magnetized and magnetized samples at increasing test times (5, 15, 20, 30, 40 and 60 days) are shown in Fig. 1, together with their standard deviations. The data presented are a mean of six samples and represent the results obtained after heat treatment at 400°C for 30 min. For all periods, the magnetized samples were associated with larger weight losses comparatively to the non-magnetized ones, with the largest differences being obtained after 5 and 60 days of immersion. The mass of the material released during the heat treatment for demagnetization of the magnetized samples was approximately 1.3% of their initial mass.

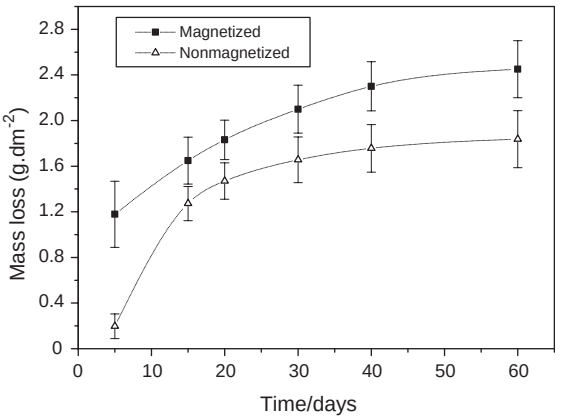

Fig. 1. Weight loss results for magnetized and non-magnetized samples after various times of immersion.

Figs. 2(a) and (b) show typical polarization curves for non-magnetized and magnetized samples at increasing immersion times, 1, 10, 30 and 60 days, in the 3.5 wt% NaCl test solution. For both types of specimens, the anodic branch, after 1 day of immersion, shows a behavior typical of activation polarization from E_{corr} until approximately -700 mV (SCE) when a change in the anodic slope occurred. For test periods longer than 1 day, and at this potential range, a clear displacement to a more active state occurred; nevertheless, the shape of the curves suggests the onset of a pseudo-passive behavior for both types of samples. From potentials above -700 mV (SCE), the current density increased rapidly with the potential, indicating the onset of a new corrosion process, which seems to be the same, irrespective of the immersion time and magnetization state. Finally, at approximately -550 mV (SCE), the anodic curve shows another change in slope to higher values (around 650 mV/decade), suggesting a process controlled either by ohmic resistance or diffusion.

Values of E_{corr} and corrosion rates (i_{corr}) obtained from the polarization curves are presented in Table 2. The values of i_{corr} were determined by extrapolating the cathodic and anodic parts of the polarization curves to E_{corr}. The results presented in Table 2 show that corrosion rates increased and corrosion potential became more negative for increasing immersion

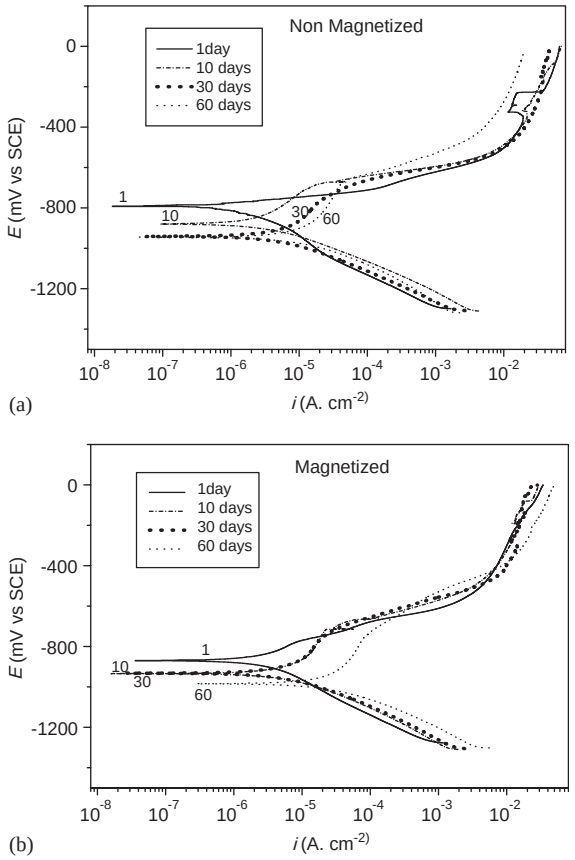

Fig. 2. Potentiodynamic polarization curves obtained for Nd–Fe–B after different times of immersion in naturally aerated 3.5 wt% NaCl solution. Scan rate: 1 mV/s. (a) Non-magnetized samples, (b) magnetized samples.

time. However, for all test times, nobler corrosion potentials and lower corrosion rates were associated to non-magnetized samples comparatively to magnetized ones. It can also be observed that the largest difference was obtained for 60 days, suggesting that the test time had a significant effect on the corrosion behavior of the magnetized specimens.

The results of EIS experiments are shown in Figs. 3 and 4 for both types of samples at increasing immersion times (1, 10, 30 and 60 days) as Nyquist and Bode diagrams, respectively. For non-magnetized and magnetized samples, Nyquist diagrams show a behavior typical of diffusion-controlled phenomena in the high-frequency (HF)

Table 2
Corrosion potentials (E_{corr}) and corrosion rates (i_{corr}) obtained from polarization curves for increasing times of immersion

Time of immersion (days)	Magnetized samples		Non-magnetized samples	
	E_{corr} (mV vs. SCE)	i_{corr} ($\mu A/cm^2$)	E_{corr} (mV vs. SCE)	i_{corr} ($\mu A/cm^2$)
1	-870 ± 35	2.5 ± 0.8	-750 ± 25	1.9 ± 0.6
10	-930 ± 47	7.0 ± 2.1	-880 ± 44	3.5 ± 1.1
30	-930 ± 42	8.0 ± 2.0	-940 ± 48	4.5 ± 1.5
60	-990 ± 54	31.0 ± 6.2	-940 ± 45	7.0 ± 2.3

Average data were obtained by three independent measurements for each condition tested. Error = ±standard deviation.

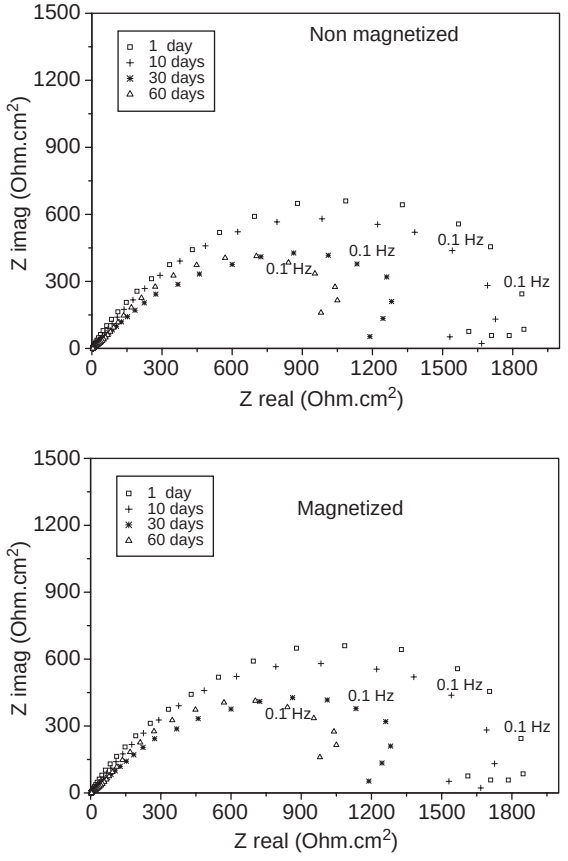

Fig. 3. Nyquist diagrams for Nd–Fe–B magnets after various times of immersion (1, 10, 30 and 60 days) in naturally aerated 3.5 wt% NaCl solution. (a) Non-magnetized samples, (b) magnetized samples.

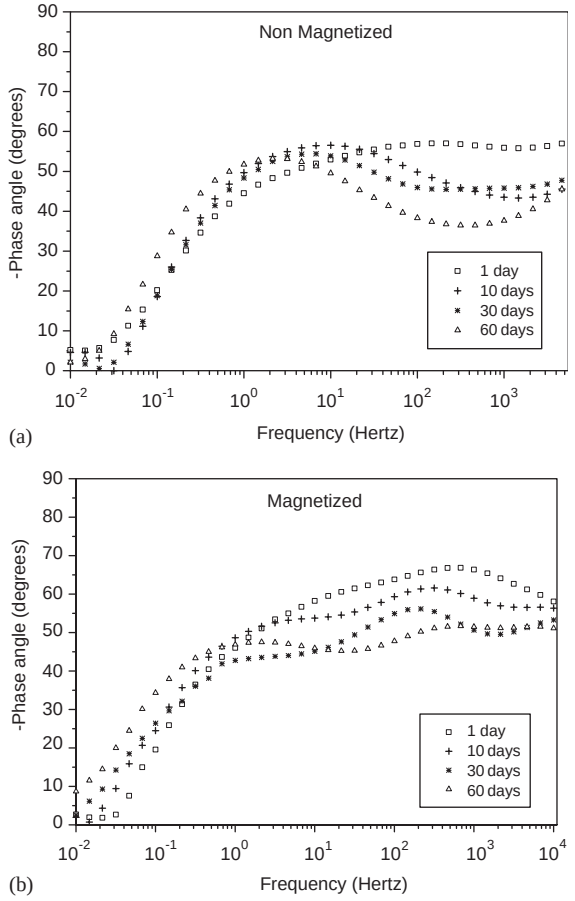

Fig. 4. Bode diagrams for Nd–Fe–B magnets after various times of immersion (1, 10, 30 and 60 days) in naturally aerated 3.5 wt% NaCl solution. (a) Non-magnetized samples, (b) magnetized samples.

region, with diagrams forming an angle of approximately 45° with the real axis. Moreover, the medium to the low-frequency region is characterized by an extremely depressed capacitive loop. Nyquist diagrams also show that magnetized samples presented a clear diminution of impedance with immersion time, while no clear

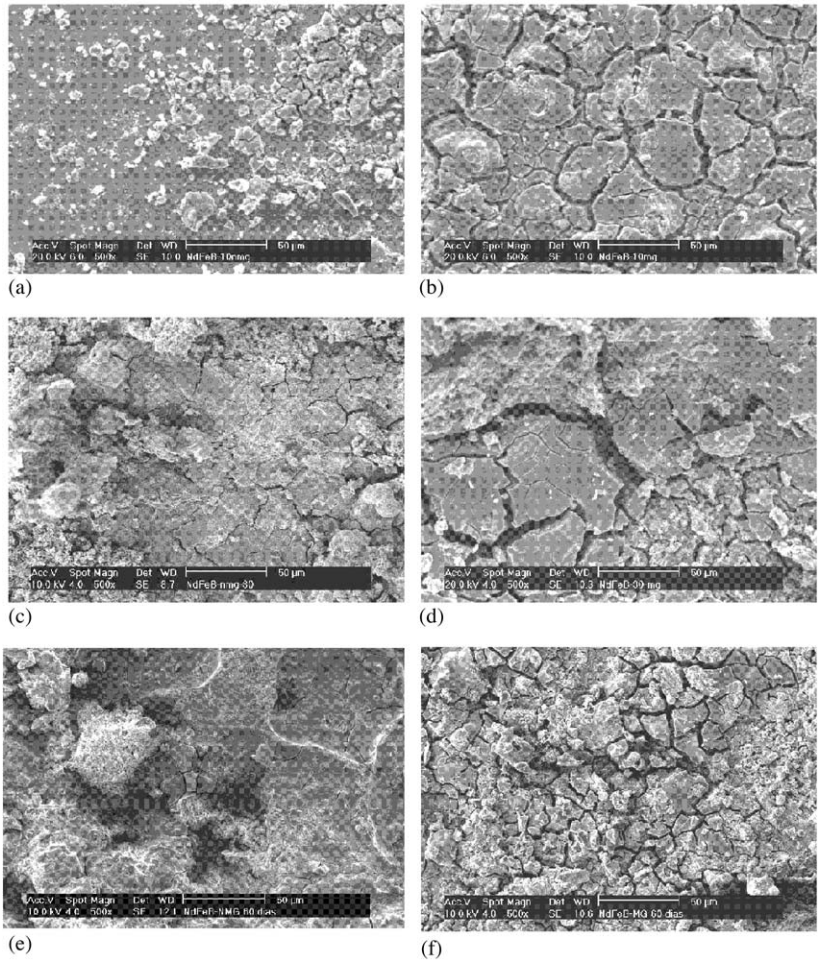

Fig. 5. SEM of Nd–Fe–B magnet surface after increasing times of immersion in naturally aerated 3.5 wt% NaCl solution. Non-magnetized samples after (a) 10 days, (c) 30 days, (e) 60 days of immersion, and magnetized samples after (b) 10 days, (d) 30 days, (f) 60 days of immersion.

tendency could be detected for non-magnetized ones. Conversely, Bode phase angle diagrams, Fig. 4, indicate a distinct behavior for the two types of samples, suggesting a dependence of the corrosion mechanism on the specimens' magnetization state. For the non-magnetized specimens, phase angles near 45° were obtained in the frequency range from 10^2 to 10^4 Hz (Fig. 4a), which slightly changed between the 10th and 60th days of immersion. This nearly constant phase-angle region is followed by a well-defined time constant in the medium to the low-frequency region.

For magnetized samples (Fig. 4b), Bode diagrams show phase angles nearly constant in a larger frequency range (from 10^4 to 1 Hz) compared to that for non-magnetized samples. However, the existence of another time constant in the higher frequency region can be envisaged, which is characterized by a shallow peak that moves towards lower frequencies with increasing immersion time.

The surfaces of the samples, either non-magnetized or magnetized, observed by scanning electron microscopy (SEM) after various test times are shown in Fig. 5. The observation of these figures

clearly shows that magnetized specimens present a greater amount of particles adhered to their surface as compared to non-magnetized ones.

Fig. 6 shows the demagnetization curves for the corrosion-tested magnets. It can be seen that corrosion decreases remanence and intrinsic coercivity of these Nd–Fe–B-type permanent magnets. Loop shape is also influenced by corrosion, but almost keeps its original shape even after 60 days of testing in the NaCl aerated solution. A summary of the magnetic properties of the corrosion-tested sintered magnets is given in Table 3. As expected, the energy product of these Nd-based permanent magnets also deteriorates with exposing time to the corrosion environment. Nonetheless, reasonable overall magnetic properties have still remained in the sintered magnets after long corrosion testing in NaCl solution.

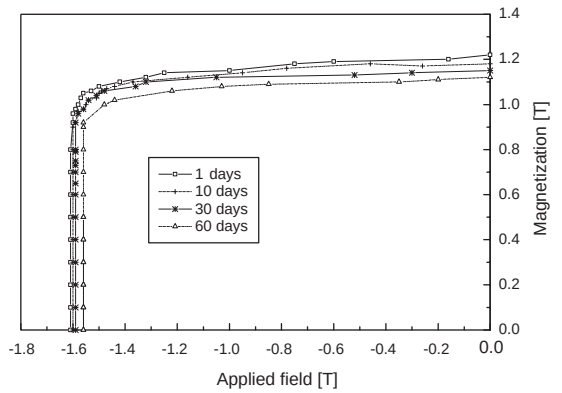

Fig. 6. Demagnetization curves of Nd–Fe–B magnets after various times of immersion in naturally aerated 3.5 wt% NaCl solution.

Table 3
Magnetic properties obtained from demagnetization curves, before and after increasing times of immersion in NaCl 3.5 wt% solution

Period	Magnetic properties		
	B_r (T) (± 0.02)	$\mu_{0i}H_c$ (T) (± 0.02)	BH_{max} (kJ m^{-3}) (± 6.0)
Before test	1.22	1.60	293
After 10 days	1.18	1.59	286
After 30 days	1.15	1.58	275
After 60 days	1.12	1.56	271

4. Discussion

4.1. Proposed explanation for the effect of the magnetic field on the oxygen transport

The much lower corrosion resistance exhibited by the magnetized specimens, compared to the non-magnetized ones, indicated by the weight loss data, mainly until 5 days of immersion, could be due to the effect of the magnetic field on the oxygen transport from the bulk solution to the magnet surface. Oxygen molecules are paramagnetic [22], and, as so, their transport towards the electrode surface must be affected by the magnetic field. It is proposed that the oxygen transport to the interface magnet/electrolyte is facilitated in the presence of the magnetic field, leading to an increased supply of these oxidizing species to the interface and consequently accelerating charge-transfer phenomena. In this assumption, when a flat magnetized surface is exposed to the electrolyte, the field would pull the oxygen flux towards the electrode surface increasing the corrosion rate. The results obtained from EIS measurements, that will be discussed later, seem to support this mechanism.

On the other hand, for longer immersion periods, the oxygen transport seems to play a minor role in the corrosion process. In this case, corrosion products attached to the specimens' surface must have been mainly responsible for the differences observed in the corrosion rates. Indeed, corrosion products were visually observed on the sample surfaces and their amount increased with time, and, as shown in Fig. 5, larger amounts of these products were associated to the magnetized specimens compared to the non-magnetized ones. The corrosion products can attenuate the effect of the magnetic field on oxygen transport. Conversely, the presence of larger amounts of attached particles to the surface of the magnetized samples would create occluded cell conditions, increasing the corrosion rate in these specimens as compared to the non-magnetized ones.

4.2. Effect of immersion time on the electrochemical response

The increase in i_{corr} for prolonged immersion times associated with E_{corr} variation to more negative values shown in the polarization curves, Fig. 2, suggest depolarization of the anodic reaction. Actually, the polarization curves indicate that immersion time mainly affected the anodic reactions, even though a pseudo-passive behavior is established for longer immersion periods. A possible reason for the increase in i_{corr} with time would be the increase in the specific area exposed to the electrolyte as corrosion proceeds. Indeed, the presence of corrosion products attached to the electrode surface, registered in the SEM micrographs presented in Fig. 5, gives support to this hypothesis, since electrolyte can penetrate through the crevices, increasing the effective area exposed to the solution. Moreover, the intrinsic porosity of the samples used in this investigation, prepared by powder metallurgy, would further contribute to expose larger surface areas to the electrolyte.

The anodic parts of the polarization curves (Fig. 2) also suggest different corrosion mechanisms related to shorter (1 day) and longer (10, 30 and 60 days) immersion periods, for both types of samples. A typical active behavior was observed for the magnets after 1 day of immersion, whereas for longer periods a pseudo-passive behavior was indicated in the potential range from E_{corr} until -700 mV (SCE). The first feature of the anodic curves can be ascribed to the preferential dissolution of the active Nd-rich phase, which is present at the grain boundaries [23]. On the other hand, the pseudo-passive behavior below –700 mV can be likely attributed to both the presence of corrosion products attached to the magnet surface and the magnets' porosity. These two features could prevent corrosion products to leave the metallic surface easily, giving rise to diffusion-controlled phenomena.

At first glance, Nyquist plots presented in Fig. 3 seem to indicate that, for shorter immersion times, the corrosion resistance of magnetized samples is higher than that exhibited by non-magnetized ones, apparently contradicting the results of weight loss experiments. However, as already stated in the results presentation, Bode phase-angle diagrams, Fig. 4, show distinct behavior for both types of samples, suggesting different corrosion mechanisms.

An analysis of Nyquist diagrams for non-magnetized samples, Fig. 3(a), seems to show no clear tendency of the impedance modulus with immersion time. This could be possibly related to the sporadic detachment of adhered particles from the specimen surface, which would periodically change the corrosion mechanism, as discussed below.

4.3. Proposal of occurrence of a diffusion-controlled process

The steady increase in current density with potential, from -700 mV (SCE) until approximately –550 mV (SCE), observed for all the anodic polarization curves, irrespective of their magnetization state or immersion time, could be related to the dissolution of the magnetic phase (ϕ phase). Indeed, Bala et al. [23] have found that the corrosion potential of the magnetic phase, in a solution of pH near to the one used in this study, was approximately –700 mV (SCE). Alternatively, the increase in the slopes observed for potentials higher than –550 mV (SCE) indicates a process controlled either by diffusion or ohmic resistance, and could be explained by a delayed diffusion of the corrosion products outwards from the porosities/crevices and from the metal surface, which would hinder the renewal of the electrolyte, preventing larger increases in corrosion rates. This could also help to explain the fairly low corrosion rates obtained from the polarization curves at the corrosion potential (order of $\mu A/cm^2$), despite the magnets' heterogeneous microstructure and their high susceptibility to corrosion. In fact, colloidal corrosion products, highly porous and not much adherent, were seen on the electrode surfaces during the performance of the experiments.

In the Bode phase-angle diagrams for non-magnetized specimens, Fig. 4(a), the presence of nearly constant phase angles, near 45°, in the high-frequency range (from 10^2 to 10^4 Hz) indicates the occurrence of a diffusion-controlled process. However, the frequency range where this phenomenon

appears is too high to be related to diffusion of species in solution. For porous electrodes, the literature [24–26] reports that HF EIS response depends on the AC signal penetrability into the pores. According to Song et al. [24], when, in a certain frequency range, the AC signal penetrates deeper than the pores length, the electrode behaves as a flat one. Alternatively, when the AC sign penetration does not reach the pore's bottom, the signal detects only the pores and phase angles between 45° and 90° can be obtained, depending on the pore's length. For non-magnetized samples, the angles near 45° at high frequencies are similar to those estimated by de Levie for diffusion in porous electrodes of semi-infinite length [27], indicating the high porosity of the samples used in this investigation, as expected for materials produced by powder metallurgy. Thus, in this frequency range, this time constant would not be related to electrochemical processes but rather to microstructural features; however, its existence evidences the main role played by porosities in the corrosion mechanism of the specimens. The variations observed in the phase angles in this frequency range can be attributed to the detachment of the particles from the surface. No clear variation of the phase angle was verified in the medium- to low-frequency region, indicating no change in the corrosion mechanism with immersion time.

4.4. Mechanism suggested for corrosion of magnetized and non-magnetized samples

Based on our experimental results for non-magnetized samples, it is proposed that corrosion occurs through a mixed process inside the pores and the crevices, where the diffusion of species can play an important role, and at the surface, due to the detachment of grains resulting from the preferential attack of the Nd-rich phase at the ϕ grain boundaries. The joint action of these two features would give rise to extremely depressed diagrams as the one obtained in the Nyquist plot. Indeed, during the performance of the experiments, pieces of the sample were frequently released from its surface. This phenomenon can be likely attributed to the detachment of Fe-rich ϕ grains from the magnet surface after large amounts of the Nd-rich phase around them have been corroded. These events would periodically expose fresh metallic area to the electrolyte, giving rise to the mixed control.

It is largely known that occluded areas like crevices and pores create ideal conditions for corrosion processes [28–30]. In these regions, large pH deviations from the bulk electrolyte occur, increasing the corrosive activity. It is likely that when the surface of the non-magnetized samples is covered with large amounts of loosely adhered ϕ grains, the corrosive activity must be higher due to the presence of large amounts of occluded areas. On the other hand, upon the detachment of the adhered particles from the surface, the exposition of fresh metal to the electrolyte would diminish the corrosive attack due to the exposure of the sample to a less corrosive condition. This cyclical mechanism would explain the apparent random change of impedance modulus with immersion time for these samples.

For magnetized samples, Bode diagrams, presented in Fig. 4(b), also exhibited a flattened phase angle in the HF region that would also be explained by the presence of porosities and crevices. However, these diagrams exhibit a time constant at high frequencies that is displaced to lower frequencies and also becomes less defined for increasing immersion time. Moreover, the flat phase-angle region expands through a wider frequency region (from 10 kHz to 1 mHz), as compared to non-magnetized samples.

From our experimental results, it is likely that the time constant at high frequencies could be explained by the effect of the magnetic field and its gradient on the transport of oxygen molecules dissolved in the solution to the interface, giving rise to higher corrosion rates for the magnetized specimens, in particular during the first few days of immersion. However, as the immersion period proceeds, the presence of attached particles to the magnet surface would reduce the influence of the magnetic field, displacing this time constant to lower frequencies (slower reactions) and diminishing the definition of the phase angle associated to oxygen-activated reactions. Indeed, demagnetization of the specimens after the immersion test

caused the release of a large amount of particles, showing that the magnetic field was responsible for their attachment to the surface even after the corrosion of the Nd-rich phase at their grain boundaries had attained a high degree.

The attachment of the ϕ particles to the magnetized sample surface would result in the penetration of corrosion perpendicularly to the surface and, consequently, a more complex crevice network would be formed, giving rise to diffusion-controlled phenomena. The observation of nearly constant 45° phase angles in the frequency range from 10^2 to 1 Hz gives support to this hypothesis. In this case, the corrosion mechanism could be very similar to that related to crevice corrosion, and the response of the electrode would be closer to that exhibited by highly porous samples.

The presence of attached particles to the magnet surface would also be mainly responsible for the higher corrosion rates exhibited by magnetized samples for longer immersion times, since it is supposed that the presence of these particles would seriously hinder the effect of the magnetic field on the oxygen transport, as indicated by the behavior of the very HF time constant. It is likely that the presence of a permanent crevice network in the magnetized samples would provide more aggressive conditions, increasing their corrosion rates.

The hypothesis proposed in this study is supported by literature results [31–33]. Le Breton and Teillet [31,32] studied the corrosion behaviour of Nd–Fe–B permanent magnets by 57Fe Mössbauer spectroscopy and X-ray diffraction, and found that oxidation occurs in the Nd-rich region and the main corrosion products are Nd_2O_3 and $Nd(OH)_3$, whereas the magnetic phase ($Nd_2Fe_{14}B_7$) is not attacked. Later, Tokuhara and Hirosawa [33] also investigated the corrosion mechanism of Nd–Fe–B sintered magnets in high-humidity environments using X-ray diffraction analysis, and found a mixture of $Nd(OH)_3$, $Nd_2Fe_{14}B_7$ and $Nd_{1+\delta}Fe_4B_4$, in the layer of powder covering the tested magnets. They attributed the corrosion mechanism of bare Nd–Fe–B sintered magnet to the selective oxidation of grain boundaries (the Nd-rich phase), to form $Nd(OH)_3$. The selective dissolution at the grain boundaries caused the $Nd_2Fe_{14}B_7$ and $Nd_{1+\delta}Fe_4B_4$ grains to come off from the bulk magnet without being seriously oxidized.

The results obtained from the demagnetization curves show that, as expected, corrosion produces an overall decrease in the magnetic properties and, surprisingly, most affected were the maximum energy product and remanence.

5. Conclusions

The results obtained by weight loss measurements, potentiodynamic polarization curves and EIS have indicated the dependence of the corrosion rates on the magnetization state of Nd–Fe–B samples produced by powder metallurgy, which at one time activates oxygen transport to the interface and retains corroded particles at the surface of magnetized samples. Higher corrosion rates and larger amounts of corrosion products adhered to the surface were related to the magnetized samples compared to the non-magnetized ones.

Due to the frequent detachment of particles from the surface of the non-magnetized samples, the corrosion mechanism for these samples was considered as being a combination of crevice corrosion and general surface attack, depending on the quantity of ϕ particles adhered to the surface. Supporting this hypothesis, Bode phase-angle diagrams have shown angles near 45° in the HF region, due to the presence of pores/crevices, while a very depressed capacitive loop was observed in the medium to low frequency due to the proposed mixed process.

Conversely, for the magnetized specimens, a more complex corrosion mechanism was proposed. For short immersion times, enhanced transport of oxygen molecules to the electrode surface, due to the action of the magnetic field, would be responsible for the higher corrosion rates exhibited by these samples. This was supported by the presence of a very HF time constant. However, for longer immersion periods, the presence of particles adhered to the surface would be the major cause of the corrosion rate due to the formation of a complex crevice network. In this latter case, Bode phase-angle diagrams tended to a flat 45° behavior typical of porous electrodes,

while the time constant at high frequencies seems to disappear.

Acknowledgements

M.C.L. Oliveira thanks CNPq for a research fellowship. The authors are also grateful to the FAPESP for financial support provided to this research.

References

[1] M. Sagawa, Trans. Jpn. Inst. Met. 23 (1982) 38.
[2] L.Z. Vorkopic, D.M. Drazic, Corros. Sci. 19 (1979) 643.
[3] A. Chiba, N. Tanaka, S. Ueno, T. Ogawa, Corros. Eng. 41 (1992) 333.
[4] A. Chiba, T. Ogawa, Corros. Eng. 38 (1989) 557.
[5] A. Chiba, K. Kawazu, O. Nakano, T. Tamura, S. Yoshihara, E. Sato, Corros. Sci. 36 (1994) 539.
[6] A. Rucinskiene, G. Biculsius, L. Gudaviciute, E. Juzeliunas, Electrochem. Commun. 4 (2002) 86.
[7] E.J. Kelly, J. Electrochem. Soc. 124 (1977) 987.
[8] J. Chopart, J. Douglade, P. Fricoteaux, A. Olivier, Electrochim. Acta 36 (1991) 459.
[9] C.-C. Lee, T.-C. Chou, Electrochim. Acta 40 (1995) 965.
[10] K. Shinohara, R. Aogaki, Electrochemistry 67 (1999) 1261.
[11] G. Hinds, J.M.D. Coey, M.E.G. Lyons, J. Appl. Phys. 83 (1998) 6447.
[12] O. Aaboubi, J.O. Chopart, J. Douglade, A. Olivier, C. Gabrielli, B. Tribollet, J. Electrochem. Soc. 137 (1990) 1796.
[13] K. Kim, T.Z. Fahidi, J. Electrochem. Soc. 142 (1995) 4196.
[14] J. Lee, S.R. Ragsdale, X. Gao, H.S. White, J. Electroanal. Chem. 422 (1997) 169.
[15] S. Mori, K. Satoh, A. Tanimoto, Electrochim. Acta 39 (1994) 2789.
[16] V. Novinski, Electrochim. Acta 42 (1997) 251.
[17] M. Waskaas, Y.I. Kharkats, J. Electroanal. Chem. 502 (2001) 51.
[18] H. Bala, S. Szymura, J.J. Wyslocki, J. Mater. Sci. 25 (1990) 571.
[19] H. Bala, S. Szymura, Appl. Surf. Sci. 32 (1998) 233.
[20] H. Bala, S. Szymura, Corros. Sci. 32 (9) (1991) 953.
[21] I. Costa, M.C.L. Oliveira, H. Takiishi, M. Saiki, R.N. Faria, Key Eng. Mater. 189–191 (2001) 340.
[22] T. Sasada, A. Sato, Phys. Lett. A 266 (2000) 350.
[23] H. Bala, G. Pawlowska, S. Szymura, Y.M. Rabinovich, Brit. Corros. J. 33 (1998) 37.
[24] H.-K. Song, Y.-H. Jung, K.-H. Lee, L.H. Dao, Eletrochim. Acta 44 (1999) 3513.
[25] H.-K. Song, H. Yong, H.K.-H. Lee, L.H. Dao, Eletrochim. Acta 45 (2000) 2241.
[26] I.V. Aoki, M.C. Benard, S.I. Cordoba de Torresi, C. Deslouis, H.G. de Melo, S. Joiret, B. Tribollet, Eletrochim. Acta 46 (2001) 1871.
[27] R. de Levie, Adv. Eletrochem. Eng. 6 (1967) 329.
[28] T. Mathiesen, E. Mahn, Adv. Powder Metall. Particul. Mater. 3 (1995) 45.
[29] L. Fedrizzi, F. Deflorian, A. Tiziani, I. Cristofolini, A. Molinari, Adv. Powder Metall. Particul. Mater. 7 (1994) 273.
[30] A. Tremblay, R. Angers, Adv. Powder Metall. Particul. Mater. 7 (1995) 274.
[31] J.M. Le Breton, J. Teillet, IEEE Trans. Magn. MAG 26 (5) (1990) 2652.
[32] J.M. Le Breton, J. Teillet, J. Magn. Magn. Mater. 101 (1991) 347.
[33] K. Tokuhara, S. Hirosawa, J. Appl. Phys. 69 (8) (1991) 5521.